Indonesian Journal of Computing, Engineering, and Design

Journal homepage: http://ojs.sampoernauniversity.ac.id/index.php/IJOCED

Deformation Behavior of Grouted Sleeve Wall Connector Under Shear Load in Precast Process of Concrete Wall

Jen Hua Ling [1], Ahmad Baharuddin Abd. Rahman [2], Izni Syahrizal Ibrahim [2]*

[1] Centre for Research of Innovation & Sustainable Development, School of Engineering and Technology, University of Technology Sarawak, 96000 Sarawak, Malaysia

[2] School of Civil Engineering, Faculty of Engineering, Universiti Teknologi Malaysia, 81310 Skudai, Johor Darul Ta'zim, Malaysia

Corresponding email: lingjenhua@uts.edu.my

ABSTRACT

This study investigated the behaviour of grouted sleeve connectors under shear loads. Tapered Head Sleeve (THS) connectors were fabricated from mild steel pipes. Five test specimens and a control specimen were produced. Each test specimen comprised two walls, which were connected by THS. An incremental shear load was applied at the joint until the specimen failed. The behaviour of the specimens was analyzed based on the load-displacement response. The feasibility of THS as a wall connection was determined based on ductility ratio, failure mode, performance ratio, and serviceability ratio. THS required an embedded length of 8 times the bar diameter to generate sufficient bond strength. The specimens experienced bar dowel action led to a significant horizontal displacement with a ductility ratio of 27.5 to 55.9. The test specimens offered shear capacities comparable to the control specimen, with performance ratios close to 1.0. The service load was only 1/3 of the ultimate capacity, and thus THS was ineffective in resisting shear load. Shear keys would be required to strengthen the joint of the specimen.

ARTICLE INFO

Article History:
Received 03 March 2022
Revised 25 May 2022
Accepted 31 Aug 2022
Available online 03 Oct 2022

Keywords:
Connection,
Grouted sleeve connector,
Precast concrete wall,
Shear load.

1. INTRODUCTION

The grouted sleeve connector is a coupler to connect steel bars (**Figure 1**). Steel bars are inserted into the sleeve to be bonded by grout. The bar-embedded length in the grout should be adequate to generate sufficient bond strength. This is to prevent the bar from slipping out of the sleeve. The connector can be used as the connection for precast concrete walls.

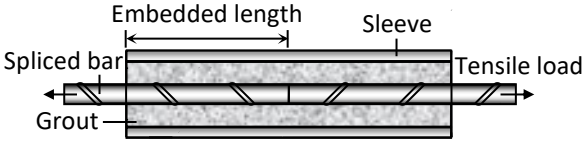

Figure 1. Grouted sleeve connector (Ling *et al.*, 2017)

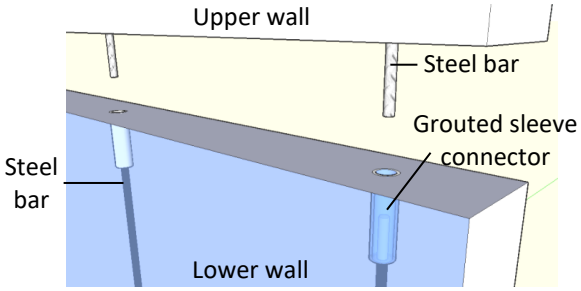

Figure 2. Grouted sleeve connector as the connection of precast concrete walls (Loh, 2008)

Grouted sleeve connectors can be embedded in precast concrete walls during fabrication, designed to receive the steel bars extruded from another wall during erection (**Figure 2**). The grout is a medium to transfer stress in the sleeve and fastens the steel bars to ensure the walls are connected. This method involves minimal wet casting, thus speeding up the construction process.

The sleeve confines the grout and controls the cracks surrounding the bars (Ling *et al.*, 2012) (**Figure 3**). This enhances the bond and shortens the bar embedded length. The embedded length typically ranges from 8.5 to 16 times the diameter of the spliced bars (Haber *et al.*, 2015). Some connectors even achieved 6 to 6.4 times the diameter of the spliced bar (Lu *et al.*, 2019). This is shorter than the conventional bar lapping system.

Another reason for the excellent bond is the high grout strength (Gao and Zhao, 2021). It creates an excellent interlocking mechanism between the grout and the bar ribs to resist the pullout force (Abd. Rahman *et al.*, 2010).

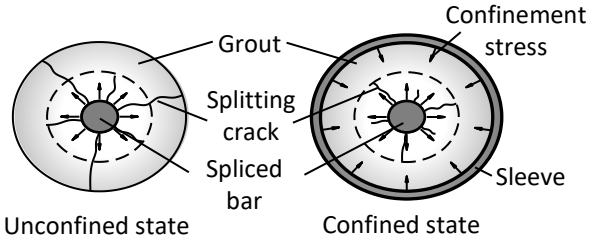

Figure 3. Effects of sleeve confinement on splitting cracks (Ling *et al.*, 2017)

Grouted sleeve connector performs well under tensile load. The performance depends mainly on the strengths and interactions of its components. This includes (a) the bar-grout bond strength, (b) the grout-sleeve bond strength, (c) the sleeve tensile strength, and (d) the bar tensile strength (Abd. Rahman *et al.*, 2010; Ling *et al.*, 2014; Sayadi *et al.*, 2014). The weakest component governs the tensile capacity (Huang *et al.*, 2017; Ling *et al.*, 2012). Ideally, a connector should have a tensile strength exceeding 1.25 times the nominal strength of the spliced bar (ACI-318, 2008; AC-133, 2008).

Grouted sleeve connectors may also be subjected to shear loads as a wall connection. A connector that is excellent in tension may not necessarily perform well under shear load (Ling *et al.*, 2017). Unlike tensile load, shear load acts perpendicularly to the connector, and the behaviour differs from those subjected to tensile load. Thus, there is a need to study the behaviour of grouted sleeve connectors under shear load.

This paper presents an experimental study of grouted sleeve connectors made of steel pipes. Due to tapered ends, the connectors were known as Tapered Head sleeves (THS). THSs performed well under tensile load (Ling *et al.*, 2012), but their performance under shear load has not been tested yet. In this study, THSs were used to connect walls subjected to shear loads, and the purpose was to evaluate their ability to resist the shear load.

2. RESEARCH METHODOLOGY

2.1. Grouted Splice Sleeve

Mild steel pipes with a nominal yield strength of 250 N/mm^2 were used to fabricate the Tapered Head Sleeve (THS). The diameters of the sleeves were 50 mm, 65 mm, and 75 mm. The sleeves were made into tapered shapes with an opening

diameter of 35 mm at both ends. The connectors had a length of 360 mm and a thickness of 4.5 mm.

THSs were used for splicing steel bars of 16 mm in diameter. The bars with a nominal yield strength of 500 N/mm^2 were embedded in the sleeve for 75 mm, 125 mm, and 175 mm lengths (**Figure 4** and **Table 1**).

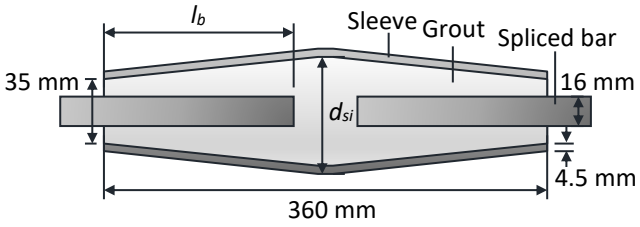

Figure 4. Tapered Head Sleeve (THS)

Table 1. Dimension of Tapered Head Sleeve (THS)

Specimen	Bar embedded length, l_b (mm)	Sleeve diameter, d_{si} (mm)
Control	-	-
THS-2	75	65
THS-4	125	50
THS-5	125	65
THS-6	125	75
THS-8	175	65

Non-shrink grout (Brand: *Sika Grout-215*) was used to fill the sleeve. It had a nominal compressive strength of 70 N/mm^2 on day 28. It was mixed into a pourable state before being poured into the sleeve. The mix proportion was 4 litres of water to 25 kg of grout.

2.2. Wall Specimens

Five test specimens and a control specimen were prepared. Each specimen comprised two walls that were separately cast (**Figure 5**). The control specimen had two steel bars extruded from the lower panel, embedded in corrugated aluminum sleeves filled with grout (**Figure 6**). The walls were cured under wet jute sacks and plastic sheets for seven days. The specimens were vertically assembled one over another. The sleeves in the lower walls were filled with grout. Then, the steel bars from the upper wall were inserted into the sleeves. After 28 days of casting, the specimens were tested with an incremental shear load.

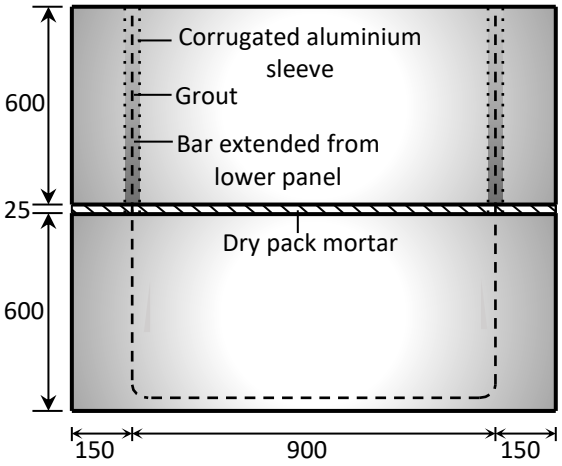

Figure 6. Control specimen (units in mm)

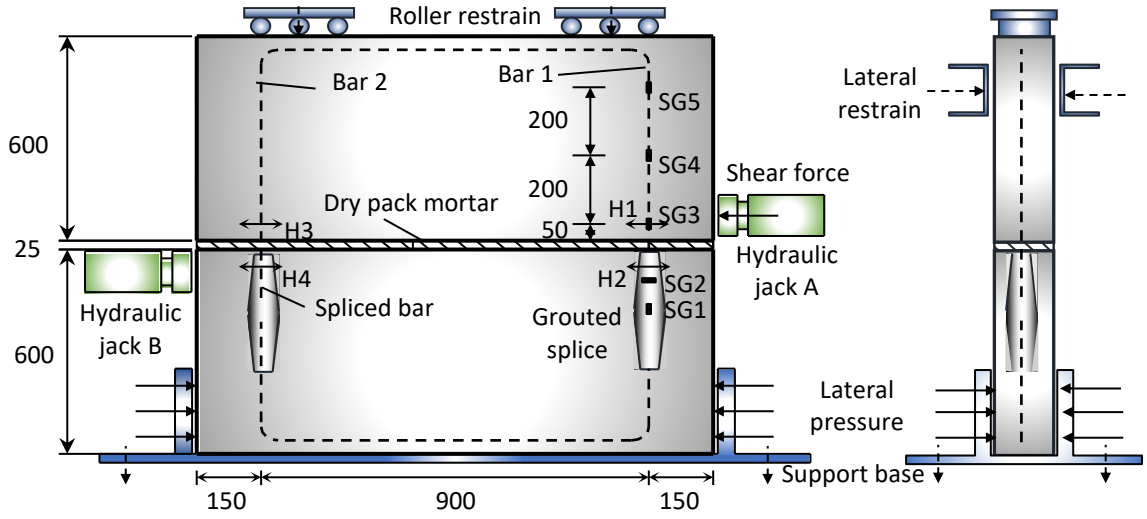

Figure 5. Details and instrumentation of wall assembly specimen (units in mm)

Details of the specimens were:

- Horizontal load: applied at the dry pack connection
- Size of walls: 1200 mm (width) x 600 mm (height) x 150 mm (thickness)
- Main and secondary reinforcements in walls: 2 layers of Y10-200 (diameter = 10 mm, spacing = 200 mm, nominal yield strength = 500 N/mm^2)
- Spliced bars: Y16 (diameter = 16 mm, nominal yield strength = 500 N/mm^2)
- Concrete: Ready-mix concrete, Grade 40, slump 75 ± 25 mm, crushed aggregate ≤ 20 mm
- Dry pack: 25 mm thickness, cement-to-sand ratio = 1:3

The test simulated the response of a wall structure subjected to lateral load. The specimens' width (1200 mm) and thickness (150 mm) resembled the typical size of a precast concrete wall. The wall height was reduced to 600 mm for easy handling in the laboratory.

2.3. Instrumentation and Test Setup

The equipment and instruments used include:

- two hydraulic jacks with the capacity of 500 kN to apply forces to the specimen
- two load cells of 500 kN capacity to measure the forces
- four linear variable differential transducers (LVDT) to measure the displacement of the specimen.
- five strain gauges (SG) to measure the elongation of the sleeve and the steel bar
- a data logger for data acquisition
- a laptop computer to monitor the data in real-time

The displacement of the specimen was measured by a series of LVDTs, H1 to H4 (**Figure 5**). The subtraction of (a) H1 and H2 and (b) H3 and H4 would be the horizontal displacements of the upper wall at Bar 1 and Bar 2, respectively.

Strain gauges were installed as follows:

- SG1 was vertically placed at the midpoint of the sleeve and was to measure the longitudinal elongation of the sleeve.
- SG2 was horizontally fixed on the sleeve and placed at the bar-embedded length's center point. It was used to measure the transverse deformations of the sleeve.
- SG3, SG4, and SG5 were installed on Bar 1. The strain gauges were used to measure the elongation of the bar at 50 mm, 250 mm, and 450 mm from the joint.

Two hydraulic jacks were placed near the dry pack joint. Hydraulic jack A induced a shear force to the upper wall. Hydraulic jack B imposed a reaction force on the lower wall. The lower wall was restrained from movement at the base. The upper wall was allowed for horizontal displacement only. Rollers and steel channels were used to prevent the lifting and out-of-plane movement of the upper wall.

2.4. Test Procedure

The test was conducted following ASTM E564. Prior to testing, all readings were set to zero. The specimen was preloaded to 10% of the estimated load for 5 minutes to consolidate the test setup. The load was then released for another 5 minutes for recovery. The process was repeated twice before the test started.

The load was progressively increased in three cycles. The load was held for at least 1 minute before the readings were taken. The load was progressively released after reaching 1/3 and 2/3 of the estimated ultimate load. Five minutes after the load was entirely removed, readings were taken. In the third load cycle, the specimen was tested until failure.

3. RESULT AND DISCUSSION

3.1. Material properties

Table 2 shows the concrete, mortar, and grout compressive strengths. These materials were used in the walls, dry pack, and sleeves, and the material samples and the wall specimens were tested on the same day.

Table 2. Compressive strength of concrete, mortar, and grout

	Compressive strength (N/mm^2)		
Specimen	**Concrete**	**Mortar**	**Grout**
Control	43.2	20.0	67.9
THS-2	46.7	33.6	63.6
THS-4	41.9	22.2	60.9
THS-5	47.0	27.8	77.6
THS-6	48.1	15.2	67.2
THS-8	44.3	30.6	61.1

Table 3 outlines the properties of steel bars under tensile load. Y10 bars were used as the primary and secondary reinforcements in the walls, and Y16 bars were spliced in THS.

In general, the quality of the materials was considered acceptable as:

a. The concrete strength achieved the design strength of 40 N/mm^2.
b. The grout strength was close to the targeted strength of 70 N/mm^2.
c. The tensile strengths of Y10 and Y16 bars were higher than the nominal strength of 500 N/mm^2.

Table 3. Properties of steel bars under tensile load

Steel bar	Sample	Yield stress (N/mm^2)	Ultimate stress (N/mm^2)	Strain (%)
Y10	A	740	777	3.6
	B	722	814	4.3
	C	678	670	4.8
Y16	A	570	667	9.7
	B	571	663	10.8
	C	560	655	10.2

The compressive strength of the mortar was inconsistent. Nevertheless, the effect on the test results would be marginal. As the shear load was applied laterally to the specimen, the dry pack was not subjected to compression.

3.2. Load-displacement response

Figure 7 presents the load-displacement responses of the specimens. The x-axis shows the displacement, while the y-axis shows the load. The curves of Bar 1 and Bar 2 were identical, and a slight variation not exceeding 0.45 mm was observed (**Table 4**). As Bar 1 was closer to the shear load, its displacement was slightly larger than Bar 2.

Table 4. Displacement test results for bar dowel action state and ultimate state

	Pre-crack state		Bar dowel action state			Ultimate state			
Specimen	**Load, P_{ic} (kN)**	**Displacement, δ_{ic} (mm)**	**Load, P_{dw} (kN)**	**Displacement at Bar 1, $\delta_{dw,b1}$ (mm)**	**Displacement at Bar 2, $\delta_{dw,b2}$ (mm)**	**Load, $P_{u,st}$ (kN)**	**Displacement at bar 1, $\delta_{u,b1}$ (mm)**	**Displacement at bar 1, $\delta_{u,b2}$ (mm)**	**Failure mode***
Control	86.4	1.2	94.7	1.69	1.44	302.6	45.7	46.1	F1
THS-2	78.3	0.5	84.1	1.01	1.03	224.1	31.6	31.6	BS
THS-4	72.2	0.8	74.8	1.03	1.08	318.5	48.9	47.2	F1
THS-5	80.8	0.6	89.4	1.23	1.23	253.6	33.8	33.9	F1
THS-6	81.9	0.6	87.4	0.80	0.81	307.2	45.6	45.0	F1, F2
THS-8	92.9	0.5	96.3	0.78	1.23	293.8	42.6	44.9	F1

Note: F1 – Fracture of Bar 1, F2 – Fracture of Bar 2, BS – Bond slip failure of Bar 1 and Bar 2

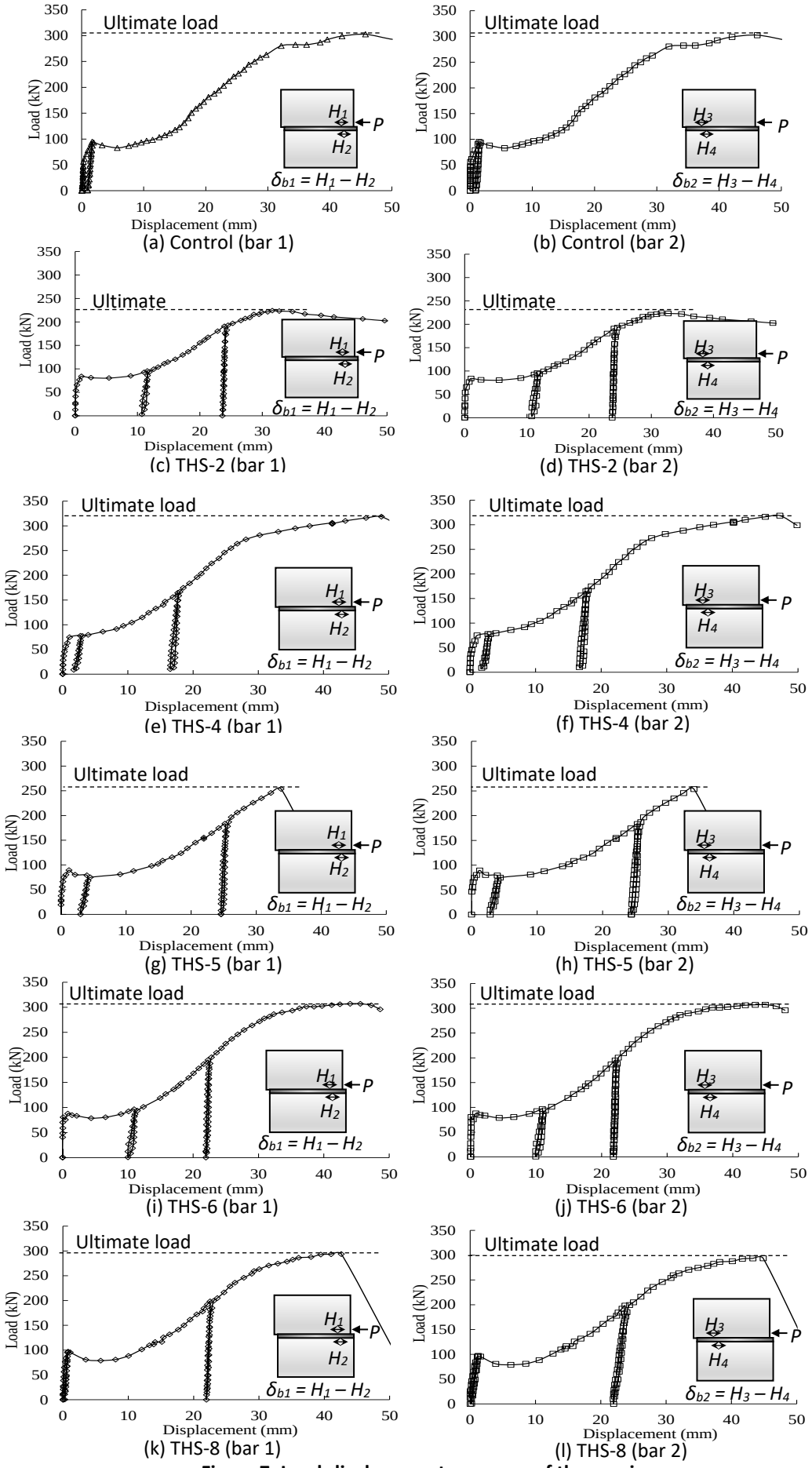

Figure 7: Load-displacement response of the specimen

The specimens exhibited a high level of ductility. The horizontal displacement can reach as high as 48.9 mm (THS-4). The specimens generally failed around 300 kN. The largest load capacity was 318.5 kN (THS-4).

Figure 8 demonstrates the typical behaviour of the specimen under shear load. The specimens went through several stages before failure. This includes pre-crack, post-crack, bar-dowel action, and post-dowel action. The bar-dowel action can be further divided into bar bending and kinking actions.

The load-resisting mechanism of the specimen varied by the stages, as described in **Table 5**. In general, the shear strength can be given by (a) the bond strength of the cold joint, (b) the interfacial friction at the cold joint, (c) the bending resistance of steel bars, and (d) the tensile resistance of steel bars.

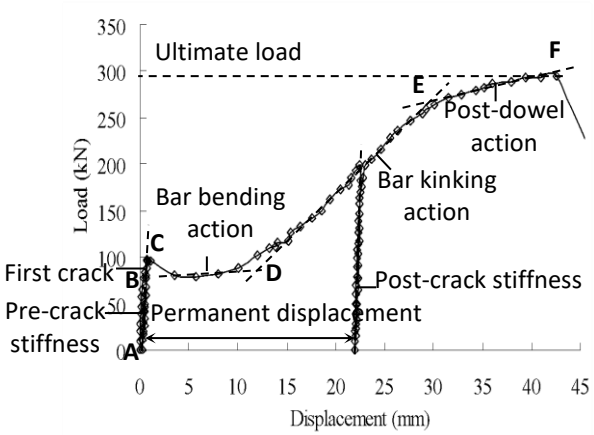

Figure 8. Behaviour of specimen under shear load (specimen THS-8)

Table 5. Stages of load-displacement response

Stages	*P-δ* curve	Description	Load resisting mechanism
Pre-crack	A-B	● Before the first cold joint crack ● The specimen resisted the shear load with good integrity. ● The high degree of stiffness ● Small horizontal displacement.	● The bond strength between the dry pack and the upper wall ● Bending strength (elastic condition) of the spliced bar
Post-crack	B-C	● A crack developed at the interface between the upper wall and the dry pack. ● Stiffness reduced marginally ● Displacement developed at a faster rate.	● Frictional resistance between the upper wall and the dry pack ● Bending strength (elastic condition) of the spliced bar
Bar bending action (bar dowel action)	C-D	● Bar 1 and Bar 2 hinged and bent at the dry pack region. ● Stiffness degraded significantly, and large displacement developed. ● The second cold joint crack developed at the interface between the dry pack.	● Bending strength (hinged condition) of the spliced bar ● Friction between the upper wall and the dry pack ● The bond strength between the dry pack and the lower wall
Bar kinking action (bar dowel action)	D-E	● Developed as the bar bending deformation reached the limit. ● Tensile stress started developing in the bar at the dry pack region. ● The specimen regained stiffness as the bars behaved elastically. ● The displacement developed proportionally to the load.	● Tensile strength of the spliced bar (elastic condition) ● Friction between the upper wall and the dry pack ● Friction between the dry pack and the lower wall
Post dowel action	E-F	● The bars yielded at the dry pack region ● Significant elongation of bar developed. ● The stiffness degraded, and considerable displacement developed.	● Tensile strength of the spliced bar (plastic condition, strain hardening) ● Friction between the upper wall and the dry pack ● Friction between the dry pack and the lower wall
Ultimate failure	Point F	● The load resistance peaked, and the specimen failed as the bar fractured or slipped out of the sleeve	● Nil (for bar fracture failure) ● Friction between the spliced bar and the grout in the sleeve (for bond-slip failure)

Figure 9 and **Table 6** explain the response of the connection under shear load. The specimen resisted the shear load with good integrity at the pre-crack stage, and stress was effectively distributed within the specimen (**Figure 9(a)**).

The first crack developed at the cold joint between the upper wall and the dry pack, triggering the frictional resistance at the joint (**Figure 9(b)**).

Then, the second crack developed at the cold joint between the dry pack and the lower wall. This happened as the spliced bar bent and hinged near the dry pack (**Figure 9(c)**). Frictional resistance developed at both cold joints as the upper wall slid horizontally.

Tensile stress developed in the splice bar during the bar kinking action, as seen in **Figure 9(d)**. It happened after the second cold joint crack. The incremental shear load was applied in three cycles. The first and second cycles stopped around 100 kN and 200 kN, respectively. The load was then progressively released until it was entirely removed. The specimens were tested for failure in the third cycle. The specimens exhibited an excellent continuity of the load-displacement curves between load cycles.

The specimen recovered to its original state before bar dowel action. Thus, negligible permanent displacement was observed after the first load cycle (**Figure 7**). The displacement was irreversible after bar-dowel action, and the bar deformed as it bent and hinged. The permanent displacement can be seen at the end of the second load cycle, and bar-dowel action greatly affected the stiffness. .

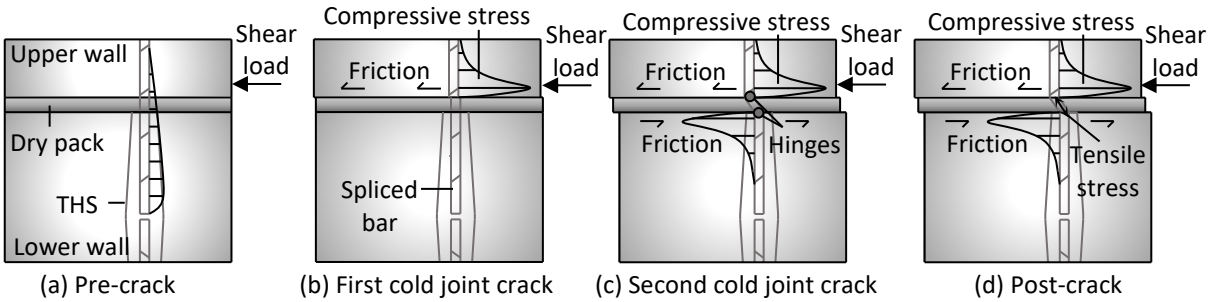

Figure 9: Response of connection under shear load

Table 6. Failure of the specimen

Failure	Cause of failure
Failure of the interfacial bond between the upper wall and the dry pack (the first crack)	● Shear load ≥ shear strength of the interfacial bond between the upper wall and the dry pack ● Horizontal displacement ≥ deformability limit of the interfacial bond
Failure of the interfacial bond between the dry pack and the lower wall (the second crack)	● Shear load ≥ (shear strength of the interfacial bond between the lower wall and the dry pack + the frictional resistance between the upper wall and the dry pack) ● Horizontal displacement ≥ deformability limit of the interfacial bond
Hinging of the spliced bar (bar bending action)	● Shear load ≥ (frictional resistance between the dry pack and the wall walls + the bending strength of the spliced bar)
Yielding of the spliced bar (post-dowel action)	● Tensile stress in the spliced bar caused by the shear load ≥ yield strength of the spliced bar
Failure of specimen	● Tensile stress in the spliced bar caused by the shear load ≥ tensile strength of the spliced bar (bar fracture failure) ● Pullout force caused by the shear load ≥ bond strength of the spliced bar.

Table 7 compares the permanent displacement at different stages. The permanent displacement would be negligible at the pre-crack stage and increase slightly at the post-crack stage, and it magnified further as it entered the bar-dowel action (i.e., bar bending and kinking actions).

Table 7. Comparative response of the permanent displacement and stiffness

Stages	Permanent displacement	Stiffness
Pre-crack	Negligible	Highest
Post-crack	Marginal	Moderate
Bar bending action	Large	Low
Bar kinking action	Very large	High

All the specimens failed by bar fracture except THS-2, which failed by bar bond slip. The fracture typically happened to Bar 1, and stress accumulated faster in Bar 1 than in Bar 2 as it was closer to the shear load. Thus, the displacements in Bar 1 were generally slightly more significant than in Bar 2 (difference ≤0.45 mm).

Specimens THS-4, THS-5, THS-6, and THS-8 failed by bar fracture. These specimens had bar embedded lengths of at least 125 mm, equivalent to 8 times the bar size. The longer the bar embedded length, the stronger the bond (Ling *et al.*, 2016; Gao and Zhao, 2021; Zhao *et al.*, 2019). When the bond strength exceeded the tensile capacity, the bar fractured.

The effect of the sleeve diameter on the performance of THS was unclear in this study. This was due to the limited number of specimens tested. Specimens THS-4, THS-5, and THS-6 had the same bar embedded length but with different sleeve diameters, and all of them failed by bar fracture. Thus, it was hard to distinguish which specimen gave a higher bond strength. Theoretically, the grouted sleeve with a smaller diameter offered a higher bond strength (Ling *et al.*, 2016; Gao and Zhao, 2021). The confinement to the grout in a small sleeve would be more effective (Ling *et al.*, 2012).

The bar-bending action commenced around 100 kN. This led to a notable structural change in the specimen. The spliced bar hinged, and the permanent displacement accumulated. This defined the service strength of the specimen. The service load should exceed 3/4 of the ultimate capacity for the best specimen performance.

The low service load led to exceptionally high ductility, which was unnecessary. For survival purposes, a specimen should exhibit warning signs before failure, and the displacement should be just enough to be visually noticeable. Further deformation would be redundant, especially when there is a considerable strength surplus.

In this case, the design strength of the connection would be limited by the service load. When the service load was 1/3 of the ultimate capacity, the unutilized strength would be double its design strength. This was rather wasteful. To overcome this, shear keys may be provided at the wall joint. The shear keys can enhance the shear strength of the joint (Soudki, 1994) (**Figure 10**). This allows the grouted sleeve connector to undertake tensile load only.

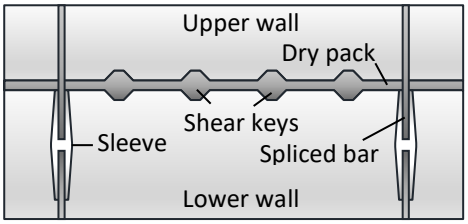

Figure 10: Shear keys for wall connection

3.3. Internal stress

Figure 11 illustrates the internal stresses generated in THS under shear load. The grout bonded with the bar to prevent it from slipping out. The sleeve

confined the grout to enhance the bond strength, and its tapered ends prevented the grout from slipping out. The sleeve connected the bars so that stress could be effectively transferred between the bars.

The ribs on the spliced bar interlocked with the grout in the sleeve. This created resultant stress acting perpendicularly to the rib surface. This resultant stress can be derived into two componential stresses:

a. The longitudinal stress interlocked with the grout, preventing the spliced bar from slipping out of the sleeve.
b. The normal stress caused the grout to expand laterally. This led to splitting cracks of grout surrounding the bar. The cracks can degrade the bond between the bar and the grout.

The transverse tensile strength of the sleeve contributed to the grout confinement, and resultant stress acted perpendicularly to the sleeve wall. The stress can also be derived into two componential stresses:

a. The longitudinal stress prevented the grout from slipping out of the sleeve.
b. The normal stress confined the grout, and it counteracted the normal stress caused by the bar ribs and controlled the splitting cracks. This improved the bond performance in the sleeve.

This study applied the shear force to the upper wall without touching the dry pack. There was an eccentricity between the shear force and the reaction force of the sleeve, and the offset distance was equivalent to the thickness of the dry pack. The spliced bar was subjected to bending due to this eccentricity, and the bending resistance of the bar resisted the shear force.

The bending stress was transferred from the bar to the grout and the sleeve. This redistributed the normal stress along the bar and the sleeve. Higher stress would concentrate at the region opposite the shear load.

The shear force acted laterally on the sleeve, leading to the sleeve's bending response. There were different regions of tension and compression in the sleeve, and the grout in the tension region might have cracked due to excessive deformation.

The stresses in the sleeve counteracted each other in a state of equilibrium. High normal stress on the spliced bar would be counterbalanced by high normal stress on the sleeve surface. The pullout force of the spliced bar was nullified by the longitudinal stresses generated in the sleeve.

The equilibrium state broke when a failure occurred. The potential failures are outlined in **Table 8**. In this study, high-strength grout and thick sleeve were used, and the failures related to the grout's compressive strength and the sleeve's tensile strength were not likely.

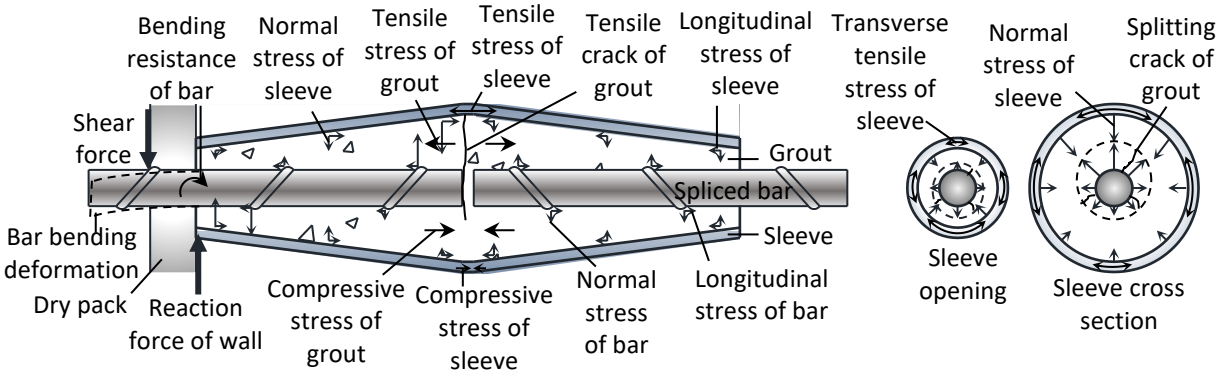

Figure 11. Internal stress in THS due to shear load

Table 8. Potential mode of failure of THS

Potential failure mode	Cause of failure
Bending deformation of bar	● Bending stress caused by the shear load > bending resistance of the spliced bar
Bending deformation of the sleeve*	● Bending stress caused by the shear load > bending resistance of the sleeve
Flexural crack of the grout due to bending deformation of the sleeve*	● flexural stress caused by the shear load > flexural resistance of the sleeve ● Bending deformation > deformability limit of the grout
Regional crushing of grout*	● Compressive stress in grout > compressive strength of grout.
Splitting crack of grout surrounding the spliced bar*	● Normal stress of bar > normal stress of the sleeve ● Peripheral tensile stress of the grout is caused by the normal stress of bar > tensile strength of the grout ● Radial expansion of the grout > deformability limit of the grout
Transverse crack of the sleeve*	● Transverse tensile stress of sleeve > transverse tensile strength of the sleeve
Bond-slip of bar	● Longitudinal stress of bar > shear strength of the grout keys that interlocked with the bar ribs
Slippage of grout*	● Pulling force caused by bar kinking action or post-dowel action > longitudinal stress of the sleeve
Bar fracture failure	● Tensile force caused by bar kinking or post-dowel action > tensile strength of the spliced bar.

**Note: The failures were unlikely due to excess sleeve thickness and grout strength.*

4. FEASIBILITY EVALUATION

The feasibility of THS as a wall connection was analysed based on a series of ratios, adopting the method used by Ling *et al.* (2021). The criteria are as follows:

a. C1: A good connection should have adequate ductility for survival purposes (ACI-318, 2008; BS8110-1, 1997). The ductility ratio, R_d, should be at least 4.0 for the low-moderate seismic region (Equation 1) (Soudki, 1994; Liu *et al.*, 2018).

$$R_d = \frac{\delta_u}{\delta_y} \geq 4.0 \quad (1)$$

where δ_u = ultimate displacement at ultimate state (mm)
δ_y = displacement at yield (mm)

b. C2: The bond strength of the sleeve should exceed the tensile capacity of the spliced bars. Thus, bar fracture failure was preferred.

c. C3: The load capacity of the specimen should be equivalent to the control specimen. The performance ratio, R_p, should be at least 1.0 (Equation 2).

$$R_p = \frac{P_u}{P_{u,c}} \geq 1.0 \quad (2)$$

where P_u = ultimate capacity of the test specimen (kN)
$P_{u,c}$ = ultimate capacity of the control specimen (kN)

d. C4: The service load should not be too low compared with the ultimate load. Thus, the serviceability ratio, R_{sv}, should be at least 0.75 (Equation 3) (Ling *et al.*, 2017).

$$R_{sv} = \frac{P_{sv}}{P_u} \geq 0.75 \quad (3)$$

where P_{sv} = service load of the specimen (kN)
P_u = ultimate capacity of the specimen (kN)

The specimens were considered feasible when all the criteria were fulfilled. Based on **Table 9**, none of the specimens was feasible, and there was at least 1 criterion not fulfilled.

Table 9. Feasibility evaluation of specimen under shear load

Criteria	C1			C2	C3			C4		Feasibility	
	δ_{dw} (mm)*1	δ_u (mm)*1	R_d	Failure mode*2	P_u (kN)	$P_{u,c}$ (kN)	R_p	P_{sv} (kN)*3	R_{sv}	Score *4	Feasible*5
Ref.	Table 4	Table 4	Eq. 1	Table 4	Table 4	Table 4	Eq. 2	Table 4	Eq. 3		
Req.			≥4.0	F			≥1.0		≥0.75		
THS-2	1.02	31.60	31.0	S	224.1	302.6	0.74	84.1	0.38	1/4	N
THS-4	1.06	48.05	45.3	F	318.5	302.6	1.05	74.8	0.23	3/4	N
THS-5	1.23	33.85	27.5	F	253.6	302.6	0.84	89.4	0.35	2/4	N
THS-6	0.81	45.30	55.9	F	307.2	302.6	1.02	87.8	0.29	3/4	N
THS-8	0.94	43.75	46.5	F	293.8	302.6	0.97	95.2	0.32	2/4	N

Notes: *[1]The average values of Bar 1 and Bar 2 were taken*
[2]F – bar fracture failure, S – bar bond-slip failure
[3]Service load, P_{sv} was considered equivalent to Pre-dowel action load, P_{dw}
[4]Score – number of criteria fulfilled / total number of criteria
[5]Y – Feasible, N – Not feasible

Criterion C4 was the most critical for THS. None of the specimens met the requirement, which was attributed to the shear load acting perpendicularly to THS. The service load remained low even if the bond strength was adequate. The service load was only 1/3 of the ultimate strength, although an adequate bar embedded length of 125 mm was provided.

5. CONCLUSION

This study tested a grouted sleeve connector known as Tapered Head Sleeve (THS). The behaviour under incremental shear load was investigated. The specimens experienced pre-crack, post-crack, bar-bending action, bar-kinking action, post-dowel action, and ultimate failure. Under shear load, stresses developed in the grout and the sleeve. The sleeve, grout, and spliced bars interacted to prevent the bar from slipping out. The wall connection experienced significant horizontal displacement with a ductility ratio of 27.5 to 55.9. It offered a comparable strength to the control specimen, with performance ratios close to 1.0. An embedded length of 8 times the diameter of the spliced bar would generate adequate bond strength.

Due to the spliced bar's low bending resistance, the THS service load was only 1/3 of its ultimate capacity. This was the main reason THS was not feasible for resisting shear load. To overcome this, shear keys should further strengthen the walls connected by THS.

ACKNOWLEDGEMENT

This work was supported by the Research Grant of Construction Industry Research Institute of Malaysia, Vot 7371.

REFERENCES

Abd. Rahman, A. B., Ling, J. H., Ibrahim, I. S. & Abd. Hamid, Z. (2010). Performance of grouted sleeve connectors subjected to incremental tensile loads. *Malaysian Construction Research Journal, Vol. 6*, 39 -55.

AC-133 (2008). Acceptance criteria for mechanical connector systems for steel reinforcing bars. *ICC Evaluation Service, Inc*.

ACI-318 (2008). Building code requirements for structural concrete and commentary. *American Concrete Institute*.

ASTM International (2006). ASTM E564-06, Standard practice for static load test for shear resistance of framed walls for buildings.

British Standards Institution (1997). BS8110-1:1997, Structural use of concrete - Part 1: Code of practice for design and construction.

Gao, Q. & Zhao, W. (2021). Experimental study on factors influencing the connection performance of grouted welded sleeves under uniaxial tensile loads. *Journal of Building Engineering, Vol. 43*, 103033.

Haber, Z. B., Saiidi, M. S. & Sanders, D. H. (2015). Behavior and simplified modeling of mechanical reinforcing bar splices. *ACI Structural Journal, Vol. 112*, 179-188.

Huang. Y., Zhu, Z., Naito, C. J. & Yi, W. (2017). Tensile behavior of half grouted sleeve connections: Experimental study and analytical modeling. *Construction and Building Materials, Vol. 152*, 96-104.

Ling, J. H., Abd. Rahman, A. B. & Ibrahim, I. S. (2014). Feasibility study of grouted splice connector under tensile load. *Construction and Building Materials, Vol. 50*, 530-539.

Ling, J. H., abd. Rahman, A. B., Ibrahim, I. S. & Abdul Hamid, Z. (2012). Behaviour of grouted pipe splice under incremental tensile load. *Construction and Building Materials, Vol. 33*, 90-98.

Ling, J. H., Abd. Rahman, A. B., Ibrahim, I. S. & Abdul Hamid, Z. (2016). Tensile capacity of grouted splice sleeves. *Engineering Structures, Vol. 111*, 285-296.

Ling, J. H., Abd. Rahman, A. B., Ibrahim, I. S. & Abdul Hamid, Z. (2017). An Experimental Study of Welded Bar Sleeve Wall Panel Connection under Tensile, Shear, and Flexural Loads. *International Journal of Concrete Structures and Materials, Vol. 11*, 525–540.

Ling, J. H., Lim, Y. T., Leong, W. K. & Sia, H. T. (2021). Effects of Adding Silica Fume and Empty Fruit Bunch to the Mix of Cement Brick. *Indonesian Journal of Computing, Engineering, and Design*, Vol. 3(1), 19-30.

Liu, H., Han, Q., Bai, Y., Xu, C. & Du, X. (2018). Connection performance of restrained deformed grouted sleeve splice. *Advances in Structural Engineering, Vol. 21*, 488-499.

Loh, H. Y. (2008). Development of grouted splice sleeve and its performance under axial tension. Master thesis, *Universiti Teknologi Malaysia*.

Lu, Z., Huang, J., Li, Y., Dai, S., Peng, Z., Liu, X. & Zhang, M. (2019). Mechanical behaviour of grouted sleeve splice under uniaxial tensile loading. *Engineering Structures, Vol. 186*, 421-435.

Sayadi, A. A., Abd. Rahman, B. A., Jumaat, M. Z. B., Johnson Alengaram, U. & Ahmad, S. (2014). The relationship between interlocking mechanism and bond strength in elastic and inelastic segment of splice sleeve. *Construction and Building Materials, Vol. 55*, 227-237.

Soudki, K. A. (1994). Behaviour of horizontal connections for precast concrete load-bearing shear wall panels subjected to reversed cyclic deformations. PhD thesis, *University of Manitoba*.

Zhao, C., Zhang, Z., Wang, J. & Wang, B. (2019). Numerical and theoretical analysis on the mechanical properties of improved CP-GFRP splice sleeve. *Thin-Walled Structures, Vol. 137*, 487-501.